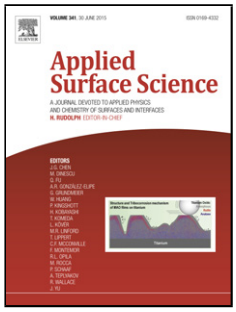

Title: Antireflection Silicon Structures with Hydrophobic Property Fabricated by Three-beam Laser Interference

Author: L. Zhao Z. Wang J. Zhang L. Cao L. Li Y. Yue D. Li

PII: S0169-4332(15)00898-3
DOI: http://dx.doi.org/doi:10.1016/j.apsusc.2015.04.058
Reference: APSUSC 30151

To appear in: *APSUSC*

Received date: 14-2-2015
Revised date: 1-4-2015
Accepted date: 7-4-2015

Please cite this article as: L. Zhao, Z. Wang, J. Zhang, L. Cao, L. Li, Y. Yue, D. Li, Antireflection Silicon Structures with Hydrophobic Property Fabricated by Three-beam Laser Interference, *Applied Surface Science* (2015), http://dx.doi.org/10.1016/j.apsusc.2015.04.058

Highlights

- A three-beam laser interference system was set up to generate periodic structures.
- Silicon surfaces were directly modified by nanosecond laser interference.
- The hexagonally-distributed hole structures can have considerably low reflectance.
- The resulting structures have a large contact angle and self-cleaning capability.
- The modulation phenomenon is not evident in three-beam laser interference.

Antireflection Silicon Structures with Hydrophobic Property Fabricated by Three-beam Laser Interference

L. Zhao[1,2], Z. Wang[1,2], J. Zhang [1], L. Cao[1], L. Li[1], Y. Yue [1,2,3], D. Li [1,2]

[1]CNM and JR3CN (Changchun University of Science and Technology), Changchun, 130022, China
[2]JR3CN (University of Bedfordshire), Luton, LU1 3JU, UK
[3]Xi'an Jiaotong-Liverpool University, Suzhou, China, 215000

Abstract—This paper demonstrates antireflective structures on silicon wafer surfaces with hydrophobic property fabricated by three-beam laser interference. In this work, a three-beam laser interference system was set up to generate periodic micro-nano hole structures with hexagonal distributions. Compared with the existing technologies, the array of hexagonally-distributed hole structures fabricated by three-beam laser interference reveals a design guideline to achieve considerably low solar-weighted reflectance (SWR) in the wavelength range of 300 nm to 780 nm. The resulting periodic hexagonally-distributed hole structures have shown extremely low SWR (1.86%) and relatively large contact angle (140°) providing with a self-cleaning capability on the solar cell surface.

Key words— Three-beam laser interference, Hexagonal structures, Antireflection, Self-cleaning, Solar cell.

1. Introduction

To fabricate solar cells with high conversion efficiency, reduction of the surface reflection is very important. Antireflection coating (ARC) technology is one of the effective methods to achieve high conversion efficiency for crystalline silicon (c-Si) solar cells [1-3]. There are currently various chemical and physical technologies used to modify or pattern silicon wafers for the fabrication of antireflection (AR) surfaces. Alkaline solutions were used to produce a random pyramid texture on crystalline silicon, and silicon nitride (SiNx) thin films were fabricated by plasma enhanced chemical vapor deposition (PECVD) [4, 5]. However, these methods have the disadvantages of complexity, high cost and more pollution. Recently, periodic subwavelength scale structures have attracted considerable attention, due to their promising antireflection properties to minimize reflection losses [6-8]. However, they are expensive, only suitable for small area or flat surface applications. Laser interference lithography (LIL) is a potential technology that can produce regular micro-nano structured patterns on silicon wafers for solar cells. This is a simple maskless low-cost and high throughput technology for producing periodic and quasi-periodic silicon structures. Up to now, many efforts have been devoted to study or fabricate micro-nano structures for different applications using LIL. Senthuran et al. reported a maskless and scalable technique for fabricating nano-scale inverted pyramid structures suitable for light management in crystalline silicon solar cells [9]. Zhang et al. fabricated periodic antireflection structures with the average reflectance of 3.5% on silicon using four-beam laser interference lithography [10]. Wang et al. proposed both antireflection and superhydrophobicity structures fabricated by direct laser interference nanomanufacturing and the contact angle and reflectance were 156.3^{o} and 5.9-15.4% [11]. Li et al. presented a method for the fabrication of highly-ordered superhydrophobic micro-nano dual structures on silicon by direct laser interference lithography [12]. The antireflection and self-cleaning functions were due to the formation of an array of micro cone and hole structures on silicon wafer surfaces. Theoretically, using four-beam laser interference method could evenly generate squarely-distributed periodic structure patterns with the antireflection and self-cleaning functions on silicon wafer surfaces, but in practice, noticeable modulations were almost unavoidably introduced in interference patterns due to the misalignment of incident angles or unequal incident angles [13], which is not desired. In contrast to four-beam laser interference, the modulation phenomenon of three-beam laser interference method is not evident, which can avoid the generation of uneven interference patterns and produce the accurate regular interference patterns to ensure the pattern consistency. In addition, the antireflection characteristics of silicon micro-nano structures, fabricated by three-beam laser interference with a hexagonally-distributed array of structures, have not been investigated. Thus, it is worthwhile to study the silicon micro-nano structures to achieve the desirable antireflection silicon structures with hydrophobic property for solar cell applications.

In this work, a three-beam laser interference system was set up to generate periodic micro-nano hole structures with hexagonal distributions. The resulting periodic hexagonally-distributed hole structures have shown extremely low SWR (1.86%) in the wavelength range from 300 nm to 780 nm and relatively large contact angle (140°) providing with a self-cleaning capability on the solar cell surface.

2. Principle

Interference patterns can be arrays or matrices of laser beam lines or dots with different periods, feature sizes and pattern shapes [14]. Fig. 1 shows the configurations of three-beam (a) and four-beam (b) laser interference, and laser beam dots are formed.

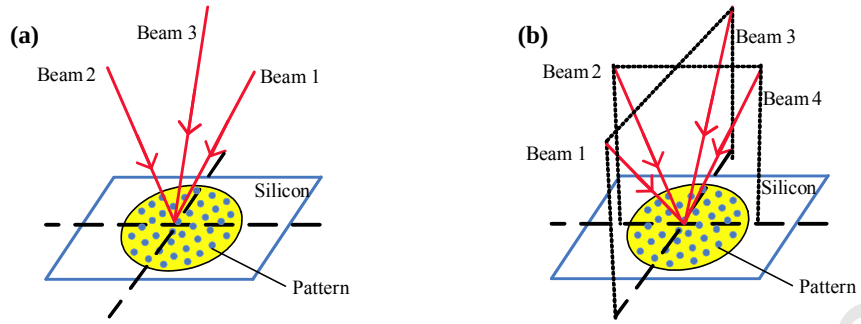

Fig. 1 Schematic diagram of multi-beam laser interference; (a) is the three-beam laser interference and (b) is the four-beam laser interference.

The multi-beam interference can be described as the superposition of electric field vectors of three or more laser beams, and it can be written as

$$\vec{E} = \sum_{i=1}^{m} \vec{E}_i = \sum_{i=1}^{m} A_i \vec{P}_i \cos(k\vec{n}_i \cdot \vec{r}_i \pm 2\pi\omega t + \phi_i) \tag{1}$$

where A_i is the amplitude, $\vec{p}_i$ is the unit polarization vector, $k = 2\pi / \lambda$ is the wave number, λ is the wavelength, $\vec{n}_i$ is the unit propagation vector, $\vec{r}_i$ is the position vector, ϕ_i is the phase constant, and ω is the frequency.

The intensity distribution of the interference pattern I can be expressed as

$$I = \sum_{i=1}^{m} |\vec{E}_i|^2 = \sum_{i=1}^{m}\sum_{t=1}^{m} |\vec{E}_i||\vec{E}_t| \cos < \vec{E}_i \cdot \vec{E}_t > \tag{2}$$

Fig. 2 shows the principles of the antireflection surface absorbing the sunlight [15].

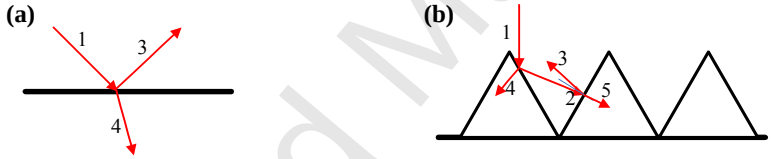

Fig. 2 The principles of the antireflection structures absorbing the sunlight. (a) is the planar surface and (b) textured surface [15].

The period of antireflection structures is defined by [16-18].

$$p < \frac{\lambda_0}{n_{air} \sin\theta_i \cos\phi + (n^2 - n_{air}^2 \sin^2\phi)^{1/2}} \tag{3}$$

where, p is the grating period, λ_0 is the vacuum wavelength, n_{air} is the air refractive index, n is the substrate material refractive index , θ_i is the polar angle of incidence light and ϕ is the azimuthal angle of incidence light.

The maximum period $P_{\max}$, when the incident light is perpendicular to the grating surface, which allows only the propagation of the zero diffraction order, is given by

$$p_{\max} = \frac{\lambda_0}{n} \tag{4}$$

It assumes that the light is incident normally on the top surface. According to the thin-film optics, as shown in Fig. 3, the condition to achieve zero reflection is

$$n_{AR-film} = (n_1 n_2)^{1/2} \tag{5}$$

$$h = \lambda / 4n_{AR-film} \tag{6}$$

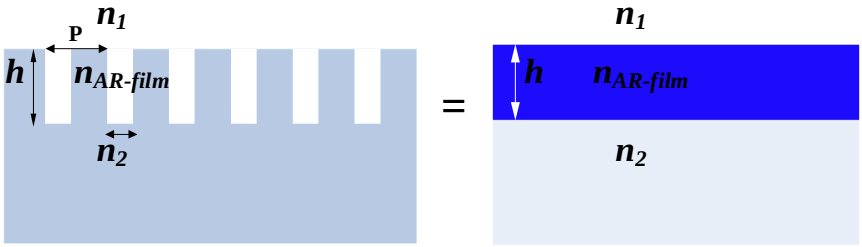

Fig. 3 Sketch of an antireflection film.

There are three theoretical models for the wetting behaviour of a water droplet on the solid surface as shown in Fig. 4. The Young model is valid in the case of a flat solid surface. The Wenzel model is used in the case of a rough surface and the liquid is in the intimate contact with the solid. The Cassie–Baxter model works in the case of the liquid rests on the tops of the asperities [19]. In this paper, the Cassie–Baxter model is used for periodic hexagonally-distributed hole structures.

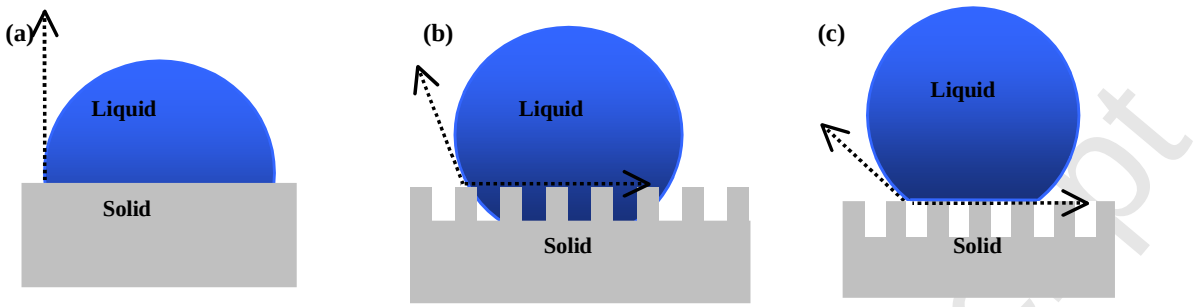

Fig. 4 Models for the wetting behavior of a water droplet on the solid surface; (a) is the Yong model, (b) is the Wenzel model and (c) is the Cassie–Baxter model.

The Cassie–Baxter model can be written as [19]

$$\cos\theta = \psi_L \cos\theta_1 + \psi_A \cos\theta_2 \tag{7}$$

θ_1 and θ_2 are the contact angles of the flat solid and air surfaces, and ψ_L and ψ_A are the solid and air surface area fractions of the solid and air surfaces.

3. Experiment

The laser interference system used a seeded Q-switched Nd:YAG laser source with the wavelength of 1064 nm, pulse duration of 7-9 ns, Gaussian beam of 6 mm in diameter and the laser fluence of 637 mJcm^{-2}. The combination of 1/4 wave plates and polarizers were used to control the pulse energy level of single beams and the polarization direction of each beam. The substrates used in the experiments were single side polished monocrystalline silicon wafers with (100) orientation. For the four-beam interference system, the laser source was divided into four beams with the same incident angles of 5.5°, the azimuthal angles of 0°, 90°, 180° and 270°, and the polarizers of 0°, 90°, 0° and 90°. For the three-beam interference system, the laser beam was divided into three beams with the same incident angles of 5.5°, the azimuthal angles of 0°, 120° and 240°, and the polarizers of 0°, 90°and 90°. After the structures fabricated on the samples, a scanning electron microscope (SEM) was used to perform the measurements of the surface morphology structures. A contact angle measurement system was used to obtain the contact angles of the silicon micro-nano structures. In order to measure the reflectance, a Xenon-lamp, a spectrograph and an integrating sphere with a detector were used.

4. Results and discussions

The results of the direct modification of silicon surface by nanosecond laser interference lithography were discussed in this section.

Laser interference fluence can produce different patterns on the silicon wafer surface with different laser parameters. The intensity distribution patterns of laser interference are dependent on the number of laser beams, the incident angles, the azimuth angles and the polarization directions. Fig. 5 shows Matlab simulation results of the two patterns obtained by three-beam and four-beam laser interference with the same incidence angles of 5.5°. For the three-beam laser interference, a hexagonally-distributed dot-like pattern is obtained and the side length of hexagonal period of intensity distributions is about 7.5 um, as shown in Fig. 5(a). For the four-beam laser interference, a squarely-distributed dot-like pattern is produced and the side length of squarely-distributed period of intensity distributions is about 8 um, as shown in Fig. 5(b).

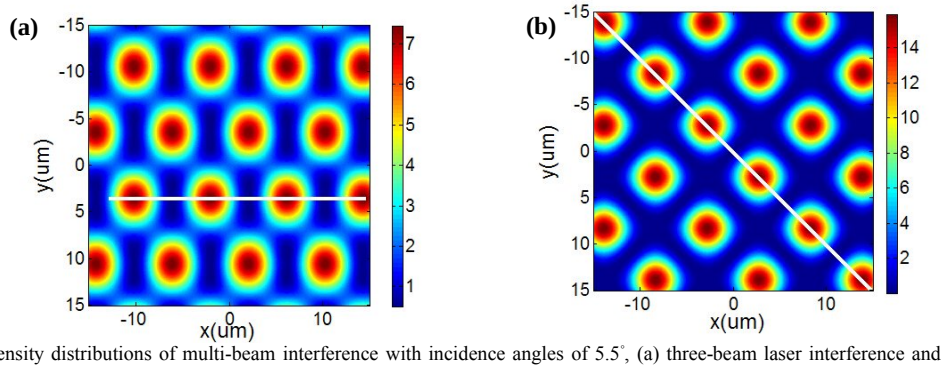

Fig. 5 Simulation of intensity distributions of multi-beam interference with incidence angles of 5.5°, (a) three-beam laser interference and (b) four-beam laser interference.

Fig. 6 shows scanning electron microscope (SEM) images of silicon micro-nano structures created by three-beam interference patterning (Figs. 6(a)-(d)) and four-beam interference patterning (Figs. 6(d)-(h)) on silicon wafer surfaces. It indicates that the different numbers of laser pulses affect the modifications of silicon surfaces by laser interference lithography, and illustrates the different topographies of structures produced by three-beam and four-beam laser interference with different laser exposures. The experimentally measured maximum periods of intensity distributions for three-beam and four-beam laser interference patterns are about 7.6 um and 9.5 um, respectively.

In previous publications of four-beam laser interference, the phenomena of secondary periodicity or modulation of the interference pattern was found in the case of slight differences between incident angles [13]. The phenomena of modulation can lead to variable sizes of features such as the shape and period of interference structures in the final pattern distribution, and the control of absolutely equal incident angles is very difficult. Comparing with four-beam laser interference, the modulation phenomenon of three-beam laser interference is not evident, which can avoid the formation of uneven interference patterns. Thus, in the case of the same incident angles, the three-beam system can produce the accurate regular interference pattern as designed.

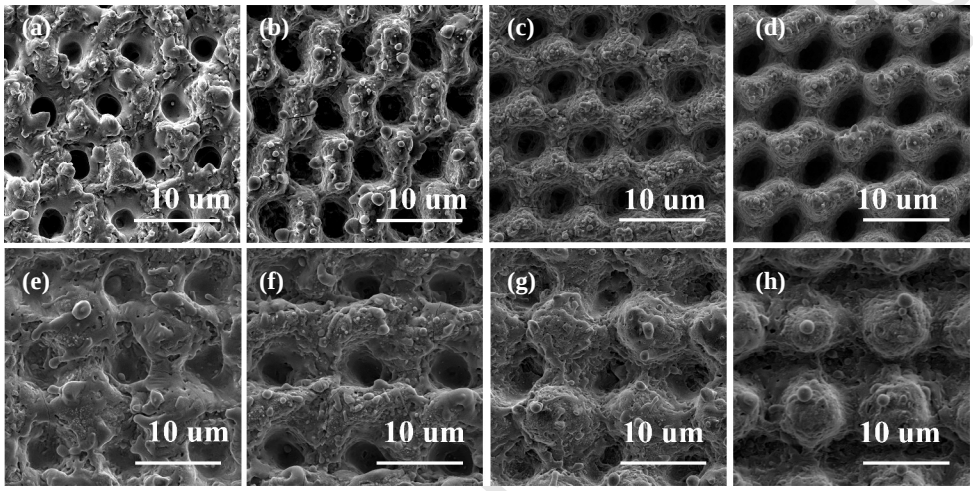

Fig. 6 (a)-(d) are SEM images of silicon structures fabricated by three-beam laser interference with a laser influence of 637 mJcm^{-2}. (a) laser exposures of 30, (b) laser exposures of 100, (c) laser exposures of 300, and (d) laser exposures of 600. (e)-(h) are SEM images of silicon structures fabricated by four-beam laser interference with a laser influence of 637 mJcm^{-2}. (e) laser exposures of 30, (f) laser exposures of 100, (g) laser exposures of 300, and (h) laser exposures of 600.

To investigate the effective reflections of the two different regular structures on silicon wafer surfaces, the light source of solar irradiation (*AM1.5G*) and the spectrograph equipped with an integrating sphere were used in the experiment [20, 21]. The solar-weighted reflectance (*SWR*) can be calculated by

$$SWR = \frac{\int R(\lambda) N_{photon} d\lambda}{\int N_{photon} d\lambda} \tag{10}$$

where $R(\lambda)$ is the reflectance, λ is the wavelength and N_{photon} is the photon number of *AM1.5G* per unit area per unit wavelength. Fig. 7 shows the measured curves of the two different regular structures. In the experiment, the laser pulses of 10, 30, 100, 300 and 600 were chosen to analyze the AR performance of the two different structures. It is observed that the reflectance of the four-beam interference fabricated pattern is higher than that of the three-beam interference fabricated pattern over the wavelength range from 380nm to 780nm.

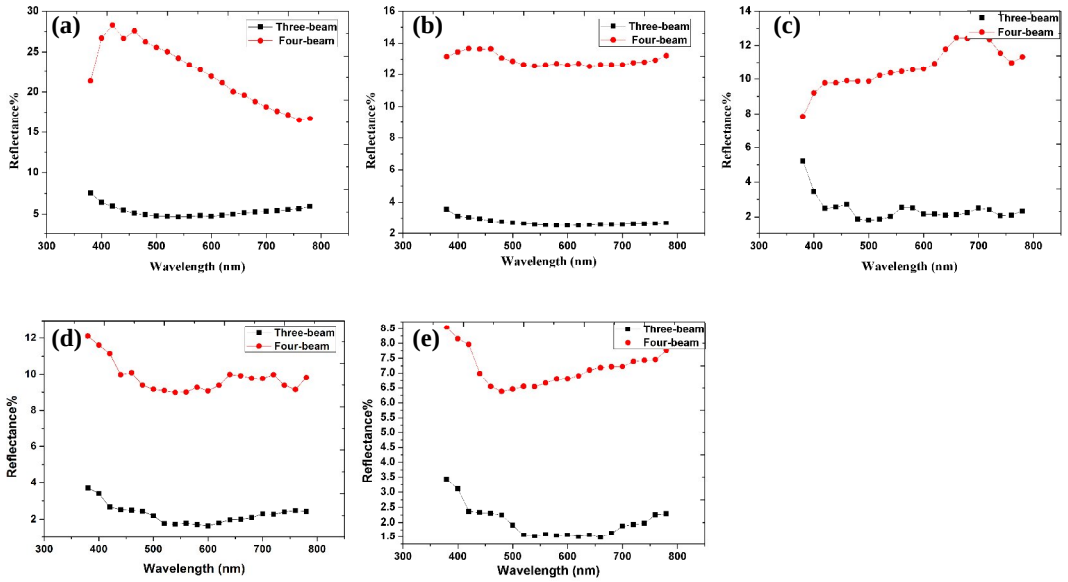

Fig. 7 Reflectance measurements of structures fabricated by three-beam (black curves) and four-beam (red curves) laser interference with the same laser influence of 637 mJcm^{-2} and the laser exposures of 10 (a), 30 (b), 100 (c), 300 (d) and 600 (e).

The laser interference exposures of 30, 50, 300 and 600 were chosen to study the optimal AR conditions. The morphology and reflectance of the samples in the visible spectrum were obtained as solar cells mainly absorbed the light in that range, as shown in Fig. 8. With the number of laser pulses increased, the SWR of the silicon hexagonally-distributed patterns was decreased from 2.6% to 1.8% in the wavelength range from 380 nm to 780 nm and the lowest SWR was obtained by the laser exposures of 600.

Due to that the highest energy distribution of sunlight is at the wavelength of 500 nm to 600 nm, which is the most concentration region of solar irradiation (*AM1.5G*), the main sunlight energy can be better absorbed by the patterns of laser exposures of 300 and 600, which are more suitable for light harvesting [21]. Hence, a proper laser exposure is required to produce desirable antireflection silicon structures that have significantly low SWR by three-beam laser interference process.

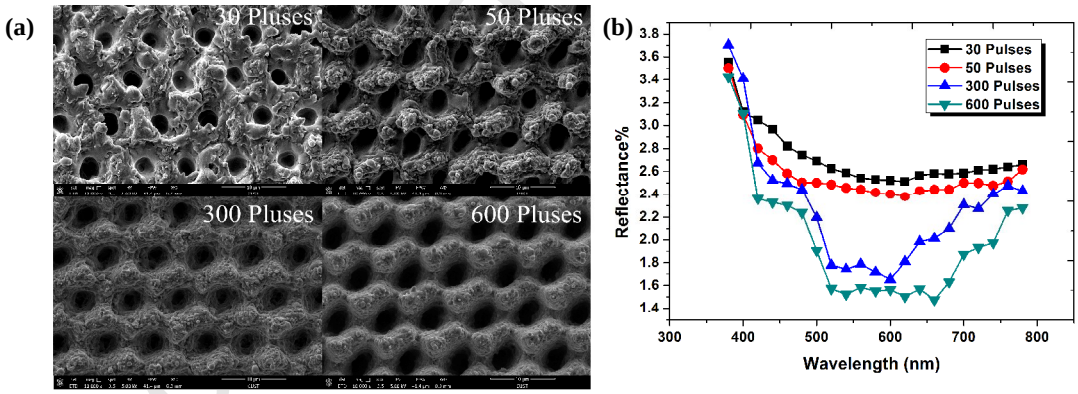

Fig. 8 The morphology (a) and reflectance (b) of regular hexagonally-distributed patterns fabricated by three-beam laser interference with different laser exposures of 30, 50, 300 and 600.

Meanwhile, the structural depth is also an important parameter for analyzing the relationship between the reflectance and the patterns. Fig .9 shows the laser exposures and the estimated average heights of the hexagonally-distributed silicon patterns as a function of calculated SWRs. With the accumulation of pulses, the structural depths tend to increase and form the better light-trapping structures. From this point of view, the number of laser exposures is also very important for obtaining a desirable surface morphology. Thus, the hexagonally-distributed pattern and appropriate structural depth can be considered as a potential candidate to produce silicon structures for solar cell applications with a low SWR value of 1.8 % in the wavelength range of 380 nm to 780 nm.

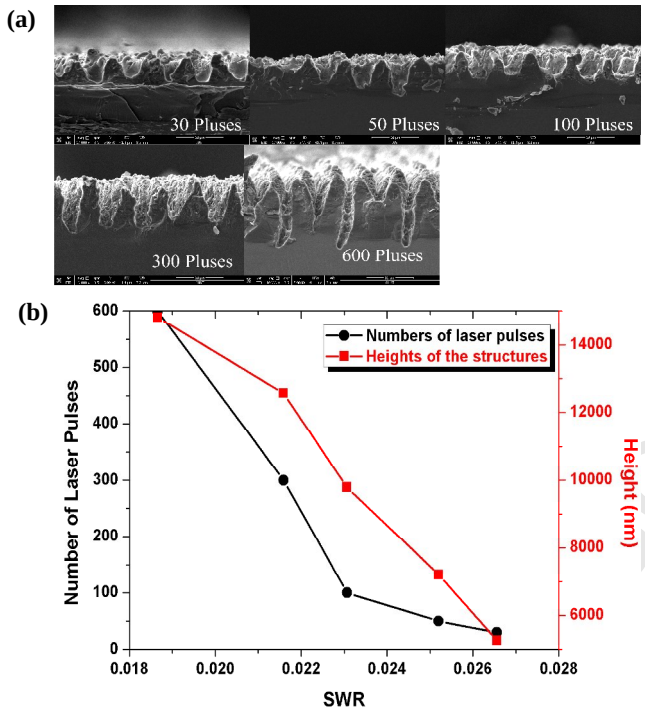

Fig. 9 (a) is the cross section SEM images of different laser pulses and the scale bar is 10 um. (b) is the laser pulses and the estimated average heights of the hexagonally-distributed silicon patterns as a function of calculated SWRs.

Fig. 10 shows the contact angle of hexagonally-distributed silicon patterns as a function of the number of pulses. (a)-(e) are water droplets with a contact angle for hexagonally-distributed patterns fabricated by three-beam laser interference with laser exposures of 30, 50, 100, 300 and 600, respectively. By comparison, the sample of optimum reflectance condition also has good hydrophobic properties. For the micro-nano roughness structures, Cassie-Baxter model is used to explain the sample surface results [19]. It is known that the hydrophobic surface offers a self-cleaning function and leads to remove the accumulated dust particles from the surface of solar cells in atmospheric environments. Thus, the crystalline silicon solar cells with antireflective structures fabricated by the three-beam laser interference process can achieve improved efficiency and realize the functions of self-cleaning and antireflection.

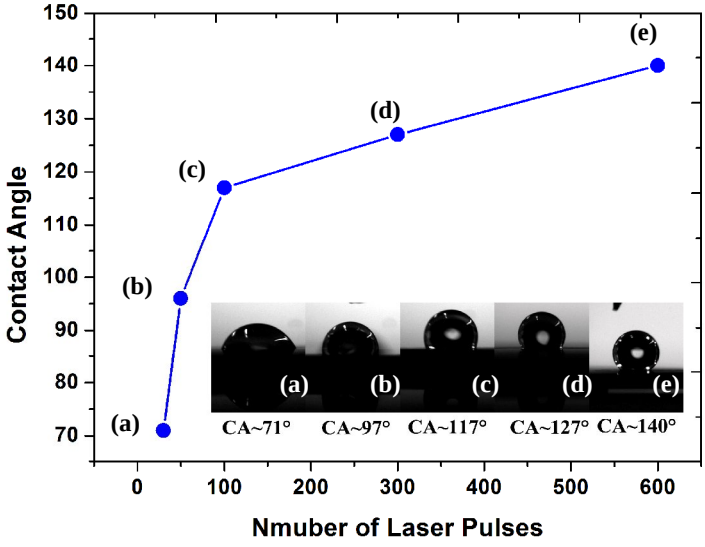

Fig. 10 The contact angles of hexagonally-distributed silicon patterns as a function of the number of pulses. (a)-(e) are water droplets with a contact angle for hexagonally-distributed patterns fabricated by three-beam laser interference with the laser pulses of 30, 50, 100, 300 and 600, respectively.

Conclusions

In this work, a three-beam laser interference system was set up to generate periodic micro-nano hole structures with hexagonal distributions. Compared with the existing technologies, the hexagonally-distributed hole structures reveal a design guideline to

achieve the low SWR in the wavelength range from 300 nm to 780 nm. The resulting periodic hexagonally-distributed hole structures have shown the low SWR (1.86%) and relatively large contact angle (140°) with a self-cleaning capability.

Acknowledgments

This work was supported by National Key Basic Research Program of China (973 Program No.2012CB326406), International Science and Technology Cooperation Program of China (No.2012DFA11070), National Natural Science Foundation Program of China (No.60940035 and No.61176002), Doctoral Program of Higher Education of China (No.20112216110002), and Jilin Provincial Science and Technology Program (No.201024, No.201115157, No.20110704 and No.20140414009GH).

References

[1] H.A. Atwater, A. Polman, Plasmonics for improved photovoltaic devices, Nature materials, 9 (2010) 205-213.
[2] K.Q. Peng, S.T. Lee, Silicon nanowires for photovoltaic solar energy conversion, Advanced Materials, 23 (2011) 198-215.
[3] C. Yeo, J.B. Kim, Y.M. Song, Y.T. Lee, Antireflective silicon nanostructures with hydrophobicity by metal-assisted chemical etching for solar cell applications, Nanoscale research letters, 8 (2013) 1-7.
[4] V.V. Iyengar, B.K. Nayak, M.C. Gupta, Optical properties of silicon light trapping structures for photovoltaics, Solar Energy Materials and Solar Cells, 94 (2010) 2251-2257.
[5] W. Sparber, O. Schultz, D. Biro, G. Emanuel, R. Preu, A. Poddey, D. Borchert, Comparison of texturing methods for monocrystalline silicon solar cells using KOH and Na_2CO_3, Proc. 3rd World Conference on Photovoltaic Energy Conversion (2003) 1372-1375.
[6] L. Dobrzański, A. Drygała, K. Gołombek, P. Panek, E. Bielańska, P. Zięba, Laser surface treatment of multicrystalline silicon for enhancing optical properties, Journal of Materials Processing Technology, 201 (2008) 291-296.
[7] K.C. Sahoo, M.K. Lin, E.Y. Chang, Y.Y. Lu, C.C. Chen, J.H. Huang, C.W. Chang, Fabrication of antireflective sub-wavelength structures on silicon nitride using nano cluster mask for solar cell application, Nanoscale research letters, 4 (2009) 680-683.
[8] K. Peng, M. Zhang, A. Lu, N.B. Wong, R. Zhang, S.T. Lee, Ordered silicon nanowire arrays via nanosphere lithography and metal-induced etching, Applied physics letters, 90 (2007) 163123.
[9] S. Sivasubramaniam, M.M. Alkaisi, Inverted nanopyramid texturing for silicon solar cells using interference lithography, Microelectronic Engineering, 119 (2014) 146-150.
[10] Z. Zhang, Z. Wang, D. Wang, Y. Ding, Periodic antireflection surface structure fabricated on silicon by four-beam laser interference lithography, Journal of Laser Applications, 26 (2014) 012010.
[11] D. Wang, Z. Wang, Z. Zhang, Y. Yue, D. Li, R. Qiu, C. Maple, Both antireflection and superhydrophobicity structures achieved by direct laser interference nanomanufacturing, Journal of Applied Physics, 115 (2014) 233101.
[12] W. Li, Z. Wang, D. Wang, Z. Zhang, L. Zhao, D. Li, R. Qiu, C. Maple, Superhydrophobic dual micro-and nanostructures fabricated by direct laser interference lithography, Optical Engineering, 53 (2014) 034109.
[13] D. Wang, Z. Wang, Z. Zhang, Y. Yue, D. Li, C. Maple, Effects of polarization on four-beam laser interference lithography, Applied physics letters, 102 (2013) 081903.
[14] Z. Wang, J. Zhang, Z. Ji, M. Packianather, C. Peng, C. Tan, Y. Verevkin, S. Olaizola, T. Berthou, S. Tisserand, Laser interference nanolithography, Proc. 3rd International Conference on Manufacturing Engineering (2008) 929-936.
[15] X. Meng, G. Gomard, O. El Daif, E. Drouard, R. Orobtchouk, A. Kaminski, A. Fave, M. Lemiti, A. Abramov, P. Roca i Cabarrocas, Absorbing photonic crystals for silicon thin-film solar cells: Design, fabrication and experimental investigation, Solar Energy Materials and Solar Cells, 95 (2011) S32-S38.
[16] M. Moharam, T.K. Gaylord, Diffraction analysis of dielectric surface-relief gratings, JOSA, 72 (1982) 1385-1392.
[17] D.H. Raguin, G.M. Morris, Antireflection structured surfaces for the infrared spectral region, Applied Optics, 32 (1993) 1154-1167.
[18] M. Motamedi, W.H. Southwell, W.J. Gunning, Antireflection surfaces in silicon using binary optics technology, Applied Optics, 31 (1992) 4371-4376.
[19] M. Nosonovsky, B. Bhushan, Roughness optimization for biomimetic superhydrophobic surfaces, Microsystem Technologies, 11 (2005) 535-549.
[20] H. Sai, Y. Kanamori, K. Arafune, Y. Ohshita, M. Yamaguchi, Light trapping effect of submicron surface textures in crystalline Si solar cells, Progress in Photovoltaics: Research and Applications, 15 (2007) 415-423.
[21] "Reference Solar Spectral Irradiance: Air Mass 1.5", retrieved http://rredc.nrel.gov/solar/spectra/am1.5/.